Annual Report for Period: 07/2008 - 06/2009
Submitted on: 06/10/2009
Principal Investigator: Grigoropoulos, Costas P.
Award ID: 0709090
Organization: U of Cal Berkeley
Submitted By:
Grigoropoulos, Costas - Principal Investigator
Title:
NIRT: Gated Transport through Carbon Nanotube Membranes

Project Participants

Senior Personnel

Name: Grigoropoulos, Costas
Worked for more than 160 Hours: Yes
Contribution to Project:

Post-doc

Name: Kim, Sangil
Worked for more than 160 Hours: Yes
Contribution to Project:
Experimental research on CNT membrane fabrication

Name: Fornasiero, Francesco
Worked for more than 160 Hours: Yes
Contribution to Project:
Experimental research on ion exclusion via the CNT membrane

Name: Friddle, Raymond
Worked for more than 160 Hours: Yes
Contribution to Project:
Experimental research on CNT membarane gating

Name: Liulevich, Valentin
Worked for more than 160 Hours: Yes
Contribution to Project:

Graduate Student

Name: In, Jungbin
Worked for more than 160 Hours: Yes
Contribution to Project:
CNT growth and membrane fabrication

Undergraduate Student

Technician, Programmer

Other Participant

Name: Bakajin, Olgica
Worked for more than 160 Hours: Yes
Contribution to Project:

She is a collaborator from UC Davis

Name: Noy, Aleksandr
Worked for more than 160 Hours: Yes
Contribution to Project:
He is a collaborator from UC Merced

Name: Colvin, Michael
Worked for more than 160 Hours: Yes
Contribution to Project:
He is a collaborator from UC Merced

Name: Sholl, David
Worked for more than 160 Hours: Yes
Contribution to Project:
He is a collaborator from Georgia Institute of Technology

Research Experience for Undergraduates

Organizational Partners

Lawrence Livermore National Laboratory

Other Collaborators or Contacts

Hyung Gyu Park, a post-doctoral researcher at Lawrence Livermore National Laboratory contributed to the research till he started a tenure track Assistant Professor position in ETH, Zurich in April 2009.

Activities and Findings

Research and Education Activities: (See PDF version submitted by PI at the end of the report)

In the second funding period the project focused on the CNT membrane fabrication as well as the study of fluidic transport and the detailed surface characterization for these membranes.

CNT growth kinetics

In the course of this work, we have investigated growth kinetics of multiwall carbon nanotube (MWCNT) arrays produced by catalytic thermal decomposition of ethylene gas in hydrogen, water, and argon mixture. We have proceeded to the fabrication of robust, flexible and durable CNT membranes using microfabrication techniques. As a replacement of the SiN matrix, we have introduced parylene. This would allow larger scale production of the membranes. We have conducted systematic experiments to optimize the catalyst preparation process enabling the growth of sub-2nm CNTs.

Functionalization of CNTs for active gating of membrane trasnport

We are devising and testing strategies for the active regulation and control of molecular selectivity and transport through carbon nanotubes using highly specific DNA-based molecular gating. Transport through the CNT pores is significantly affected by the chemical functionalities at the CNT pore entrance. We have investigated the presence of ionizable groups using chemical force microscopy titration experiments. The basic concept behind these measurements is to use the pH-dependent interaction forces between the surface and a chemically-modified AFM probe tip to detect changes in the ionization state of the surface chemical functionalities. Typically, these measurements also allow determination of the surface pKa in a manner analogous to conventional titration experiments.

Findings: (See PDF version submitted by PI at the end of the report)

CNT growth and Nanofluidic Membrane Fabrication
The MWCNT growth rate exhibits a non-monotonic dependence on total pressure and reaches a maximum at similar to 750 Torr of total pressure. Water concentrations in excess of 3000 ppm lead to the decrease in the observed growth rate. Optimal pressure and water concentration combination results in a reliable growth of well-aligned MWCNT arrays at a maximum growth rate of similar to 30 mu m/min. These MWCNT arrays can reach heights of up to 1 mm with typical standard deviations for the array height of less than 8% over a large number of process runs spread over the time of 8 months. Nanotube growth rate in this optimal growth region remains essentially constant until growth reaches an abrupt and irreversible termination. A quantitative model shows how accumulation of the amorphous carbon patches at the catalyst particle surface and the carbon diffusion to the growing nanotube perimeter causes this abrupt growth cessation. The influence of the partial pressures of ethylene and hydrogen on the ethylene decomposition driving force explains the nonlinear behavior of the growth rate as a function of total process pressure. This work is described in the attached paper.

Ion transport through CNT membranes
Important new understanding has been gained with respect to the transport of ions through sub-2nm CNTs. To mimic the charged groups at the selectivity region, we introduced negatively charged groups at the opening of the carbon nanotubes by plasma treatment. Pressure-driven filtration experiments, coupled with capillary electrophoresis analysis of the permeate and feed, were used to quantify ion exclusion in these membranes as a function of solution ionic strength, pH, and ion valence. We showed that carbon nanotube membranes-exhibit significant ion exclusion that can be as high as 98% under certain conditions. Our results strongly support a Donnan-type rejection mechanism, dominated by electrostatic interactions between fixed membrane charges and mobile ions, whereas steric and hydrodynamic effects appear to be less important.

Training and Development:

The project provides opportunities to the post-doctoral and graduate students involved for training in the fabrication of MEMS compatible nanofluidics based on carbon nanotubes. These are utilized for studies of fluidic, ionic and gas transport through sub-2 nm pores. This is a new domain of academic research with interdisciplinary nature.
Training of underrepresented minority students has began through the SUPERB program at UC Berkeley.

Outreach Activities:

Journal Publications

F. Fornasiero, H-G. Park, J. K Holt, M. Stadermann, C. P. Grigoropoulos, A. Noy, O. Bakajin,, "Ion Exclusion by sub 2-nm Carbon Nanotube Pores", Proc. Natl. Acad. Sci. USA, p. , vol. , (2008). Accepted,

A. Noy, H.-G. Park, F. Fornasiero, J. K. Holt, C. P. Grigoropoulos, O. Bakajin, "Nanofluidics in Carbon Nanotubes", Nano Today, p. 22, vol. 2, (2007). Published,

Stadermann, M., Sherlock, S.P., In, J.B., Fornasiero, F., Park, H.G., Artyukhin, A.B., Wang, Y., DeYoreo, J.J., Grigoropoulos, C.P., Bakajin, O., Chernov, A.A., and Noy, A, "Length Control, Catalyst Poisoning, and Kinetics of CVD Growth of Multi-wall Carbon Nanotube Arrays", Nano Letters, p. 738, vol. 9, (2009). Published,

Books or Other One-time Publications

OLGICA BAKAJIN, ALEKSANDR NOY,
FRANCESCO FORNASIERO1 COSTAS P.
GRIGOROPOULOS, JASON K. HOLT,
JUNG BIN IN, SANGIL KIM, HYUNG GYU
PARK, "Nanofluidic Carbon Nanotube
Membranes: Applications for water
purification and desalination", (2009). Book, Accepted
Editor(s): Diallo, Duncan, Savage, Street
Collection: Nanotechnology Applications: Solutions
for Improving Water Quality
Bibliography: William Andrew Publishers

Web/Internet Site

Other Specific Products

Contributions

Contributions within Discipline:

We have accomplished the first demonstration of ion exclusion through nanoscale pores. We have also conducted a series of experiments on the transport of gases and mixtures of gases through the nanoscale CNT pores. We have also achieved good control of the sub-2 nm SW AND DW CNT size, uniformity and growth rate by enginnering the catalyst and the reactor flow and temperature conditions.

Contributions to Other Disciplines:

The project is of interdisciplinary nature, combining chemistry, physics, computational simulation development, experimental and theoretical studies of fluidic transport phenomena
and microdevice fabrication.

Contributions to Human Resource Development:

As previously noted, the project provides an entirely new domain for the training of graduate students and post-docs on the study of transport through pores of size commensurate with the molecular dimensions. This offers unprecedented possibilities for fast transport with many important consequences for example in desalination, water treatment, osmotic power generation and alternative membranes for energy devices.

Contributions to Resources for Research and Education:

We have built experimental setups for the study of fluidic transport through CNT membranes, the fabrication, testing and characterization of CNT nanofluidics. New computational methods are being developed for the transport of gases through nanoscale pores.

Contributions Beyond Science and Engineering:

Conference Proceedings

Special Requirements

Special reporting requirements: None
Change in Objectives or Scope: None
Animal, Human Subjects, Biohazards: None

Categories for which nothing is reported:

Activities and Findings: Any Outreach Activities
Any Web/Internet Site
Any Product
Contributions: To Any Beyond Science and Engineering
Any Conference

Nanofluidic Carbon Nanotube Membranes:

Applications for water purification and desalination

OLGICA BAKAJIN[1,*], ALEKSANDR NOY[1,*], FRANCESCO FORNASIERO[1] COSTAS P. GRIGOROPOULOS[2], JASON K. HOLT[1], JUNG BIN IN[1,2], SANGIL KIM[1], HYUNG GYU PARK[1]

[1]Molecular Biophysics and Functional Nanostructures Group
Chemistry, Materials, Earth, and Life Sciences Directorate,
Lawrence Livermore National Laboratory, Livermore, Ca 94550

[2]Department of Mechanical Engineering
University of California at Berkeley, Berkeley, Ca 94720

[*]**E-mail**: *bakajin1@llnl.gov, noy1@llnl.gov*

Abstract

Unique geometry and internal structure of carbon nanotubes give rise to a newly discovered phenomena of ultra-efficient transport of water through these ultra-narrow molecular pipes. Water transport in nanometer-size nanotube pores is orders of magnitude faster than transport in other pores of comparable size. We discuss the basic physical principles of the ultra-efficient transport in carbon nanotubes, the fabrication of carbon nanotube membranes, and their nanofiltration and ion exclusion properties. A rare combination of transport efficiency and selectivity makes carbon nanotube membranes a highly promising technological platform for the next-generation desalination and water purification technologies. We discuss the potential for these application for improving water quality.

Nanofluidic Carbon Nanotube Membranes:

Applications for water purification and desalination

OLGICA BAKAJIN[1,*], ALEKSANDR NOY[1,*], FRANCESCO FORNASIERO[1] COSTAS P. GRIGOROPOULOS[2], JASON K. HOLT[1], JUNG BIN IN[1,2], SANGIL KIM[1], HYUNG GYU PARK[1]

[1]Molecular Biophysics and Functional Nanostructures Group
Chemistry, Materials, Earth, and Life Sciences Directorate,
Lawrence Livermore National Laboratory, Livermore, Ca 94550

[2]Department Of Mechanical Engineering
University of California at Berkeley, Berkeley, Ca 94720

[*]**E-mail**: *bakajin1@llnl.gov, noy1@llnl.gov*

1. Introduction: Carbon nanotube membrane technology for water purification.

Availability of safe, clean and inexpensive water has emerged as an issue that defines global problems in the 21st century. Water shortages are some of the root causes of the societal disruptions such as epidemics, environmental disasters, tribal and ethnic conflicts, growth shortfalls, and even country-wide political destabilization. Membrane-based filtration is the current leading energy-efficient technology for cleanup and desalination of brackish water, recycled water, and seawater. Membrane-based filtration offer other advantages as filtration through the tight membrane pores can also remove dangerous impurities, such as *As*, as well as dangerous large organic compounds. Factors that limit the efficiency of the membrane purification technologies include the membrane resistance to the flow, membrane fouling, and membrane imperfections that lead to incomplete rejection or in the drop of the membrane rejection properties overtime. Latest technological developments and in particular high efficiency energy recovery systems have pushed the current efficiency of the RO membranes to a very impressive 4kWh/m^3 [1]; however, this number is still above the theoretical minimum energy cost of 0.97kWh/m^3 for 50% recovery [2, 3]. To move further we need to develop transformative membrane technologies that utilize fundamentally new transport and filtration mechanisms for drastic gains in transport efficiency.

Carbon nanotube membranes are a promising candidate for one such solution primarily because of their transport charscteristics. The inner cavity of carbon nanotube forms a natural pore with very small diameter that can in some instances be smaller than 1 nm. Moreover, smooth hydrophobic surfaces of the nanotubes lead to nearly frictionless flow of water through them that enables transport rates that are orders of magnitude higher than transport in conventional pores. Finally, structure of carbon nanotubes permit targeted specific modifications of the pore entrance without destroying the unique properties of the inner nanotube surface. The combination of these three factors could enable a new generation of membranes whose transport efficiency, rejection properties and lifetimes drastically exceed those of the current membranes.

This chapter presents a brief overview of the basic physical processes that govern structure and transport of water inside carbon nanotube pores, basic properties that make nanotube pore technologies attractive for water purification and desalination, the fabrication approaches for producing carbon nanotube membranes, and the experimental observations of water transport and ion exclusion properties in CNT membranes.

2. Basic structure and properties of carbon nanotubes.

By now carbon nanotube (CNT) has firmly established itself as the iconic molecule of nanoscience [4]. A carbon nanotube is simply a nanometer-sized rolled-up atomically-smooth graphene sheet that forms a perfect seamless cylinder (Figure 1) capped at the ends by fullerene caps. It is common to characterize the structure of the nanotube by its rolled-up vector (*n*,*m*), called chirality or helicity, which defines the position of the matched carbon rings during the roll-up of the graphene sheet [5]. A carbon nanotube can have one (as in case of a single-walled carbon nanotube), or several concentric graphitic shells (as in case of multi-walled nanotubes) and it can reach up to several millimeters in length, yet retain a diameter of only a few nanometers.

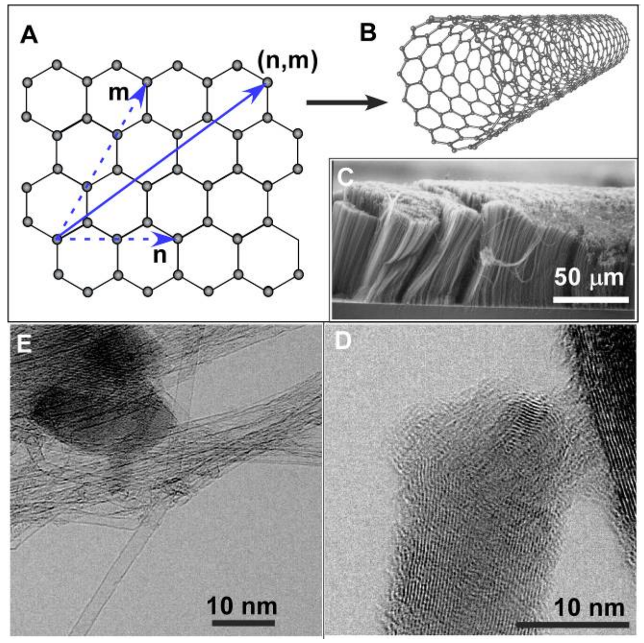

Figure 1. **Structure and morphology of carbon nanotubes. A**. Schematic representation of a grapheme sheet and a carbon nanotube roll-up vector. The roll-up vector is perpendicular to the axis of carbon nanotube. **B**. A 3-D model of a single-wall carbon nanotube. **C**. An SEM image of a vertically-aligned array of multi-wall carbon nanotubes grown on a silicon substrate. (SEM images: M. Stadermann, O. Bakajin, A. Noy, LLNL) (**D,E**) TEM images of single-wall (E) and multi-wall (D) carbon nanotubes. (TEM images: J. Plitzko, A. Noy, LLNL)

Several methods of CNT production currently exist. In the laboratory environment catalytic chemical vapor deposition (CVD) is preferred over other methods such as arc discharge and laser ablation because it produces higher quality carbon nanotubes. CVD reactors can produce individual isolated nanotubes, as well as densely packed vertically-aligned arrays (Figure 1C). Unfortunately, the ultimate goal of the carbon nanotube synthesis- producing a uniform population of nanotubes with a given chirality- still remains elusive. Several studies indicated that the size of the catalyst particle during the growth stage determines the size of the carbon nanotube to less than 10% [6]; yet the efforts to control the size of the carbon nanotubes with greater precision have been largely unsuccessful. Thus, synthesizing a vertically-aligned carbon nanotube array with a narrow distribution of sizes still remains a difficult endeavor requiring considerable process development and optimization efforts [6-8]. The task of describing the details of CNT synthesis goes well beyond the scope covered in this chapter; therefore we refer the readers to a number of reviews on this subject [9-11].

3. Water transport in carbon nanotube pores: an MD simulation view.

3.1 Water inside carbon nanotubes. The task of observing and understanding fluid and gas flows in carbon nanotube pores raises a set of unique fundamental questions [12]. First, it is surprising that hydrophilic liquids, especially water, enter and fill very narrow and hydrophobic carbon nanotubes. If the water does enter the carbon nanotubes, what influence does extreme confinement have on the water structure and properties? It is important to evaluate how these changes in structure influence the rates, efficiency and selectivity of the transport of liquids and gases through the carbon nanotubes. As it is often the case, molecular dynamics simulations have provided some of the first answers to these questions. G. Hummer and colleagues used MD simulations to observe (Figure 2A,B) filling of the (6,6) nanotube (0.81 nm in diameter and 1.34 nm in length) with water molecules [13]. Surprisingly, they found that water filled the empty cavity of the carbon nanotube within a few tens of picoseconds and the filled state continued over the entire simulation time (66 ns). More importantly, the water molecules confined in such a small space formed a single-file configuration that is unseen in the bulk water. Several experimental studies also provide some evidence of water filling of carbon nanotubes [14-17]. Further analysis of the simulation results Hummer and colleague showed that water molecules inside and outside the nanotube were in thermodynamic equilibrium. This observation illustrates one of the more important and counterintuitive phenomena associated with the nanofluidic systems: nanoscale confinement leads to the narrowing of the interaction energy distribution, which then causes the lowering of the chemical potential [13]. In other words, confining the liquid inside a nanotube channel actually lowers its free energy! Further simulations by the same group showed that the filling equilibrium was very sensitive to the water-nanotube interactions parameters: a 40% reduction in the depth of the carbon-water interaction potential resulted in the emptying of the carbon nanotube cavity, or a 25% reduction resulted in the fluctuation between filled- and empty states (bi-stable states) [13, 18]. This sharp transition between the two states has been observed for other hydrophobic nanopores as well [19, 20 , 21, 22]. MD simulations have also studied the dependence of the carbon nanotube hydration on other properties of carbon nanotubes such as the nanotube wall flexibility [23], charge [24, 25], chirality [25, 26], length [18], and diameter [24, 27, 28].

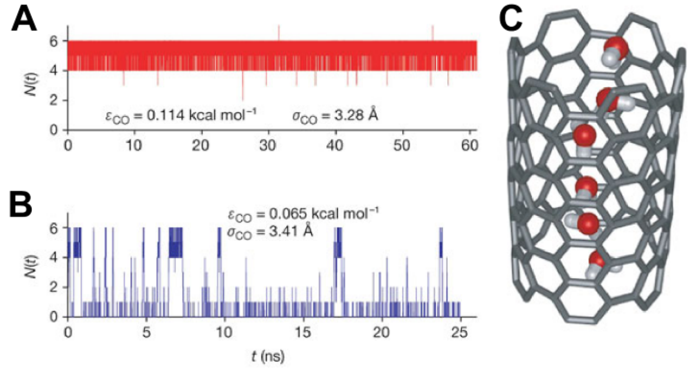

Figure 2. **MD simulations of water and proton transport in carbon nanotubes. (A,B)**. Number N of water molecules inside an 8.1Å diameter nanotube as a function of time for sp^2 carbon parameters (A) and reduced carbon–water attractions (B). (**C**) Structure of the hydrogen-bonded water chain inside the carbon nanotube. Reproduced from [13] with permission © 2001 Nature Publishing Group.)

3.2 Carbon nanotubes as biological channel analogs. MD simulations show that a defining feature of the water structure in carbon nanotubes is the formation of the hydrogen-bonded "water wires" (Figure 2C) oriented along the nanotube axis [12, 13, 29]. Such one-dimensional hydrogen bonded structures are highly reminiscent of the "water wires" observed in the biological channels specializing in water transport, such as aquaporins [30]. In fact, the similarity between aquaporin channels and carbon nanotube channels goes further. Similar to the hydrophobic interior of carbon nanotubes, the inner cavity of the aquaporins is lined with hydrophobic residues that facilitate the formation of the one-dimensional hydrogen-bonded water chains [30, 31]. Weak interactions of water molecules with the hydrophobic walls combine with the smooth nature of the nanotube walls to enable nearly-frictionless transport of water in nanotubes channels. Kalra and Hummer et. al. showed that water moves very rapidly through a nanotube channel under osmotic pressure [29]. They observed that friction at the channel walls in that system was so low that water transport was no longer governed by the Hagen-Poisselle flow, but instead depended mainly on the events at the nanotube entrance and exit [29]. As the result calculated rates of water transport approached 5.8 water molecules per ns per nanotube. Interestingly, these rates are comparable to the water transport rates achieved in aquaporins [32]. Other MD simulations also observed fast water transport through carbon nanotubes [33-35].

4. Fabrication of Carbon Nanotube Membranes.

Test of these seemingly exotic predictions of fast transport through CNTs that had emerged from the MD simulations required fabrication of a robust test platform: a *carbon nanotube membrane*. Such membranes typically consist of an aligned array of CNTs encapsulated by a filler (matrix) material, with the nanotube ends opened at the top and bottom. While there are likely many ways to produce a structure of this type, (a notable early result by Martin and co-workers was based on fabrication of amorphous carbon nanotubes within porous alumina membrane template [36]), the approach that has proved most fruitful to date involves growing an aligned array of CNTs, followed by infiltration of a matrix material in the gaps between the CNTs (Figure 3A). Extremely high aspect ratio of the gaps between the nanotubes in the array (of order 1000 length/diameter or larger) presents a great fabrication challenge for this approach. Fortunately, researchers have developed successful strategies to overcome this challenge.

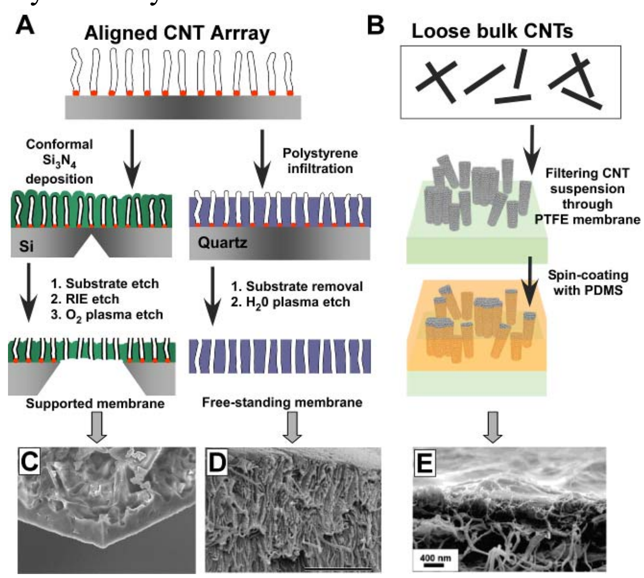

Figure 3. **Fabrication of carbon nanotube membranes.** (A, B) Process flow diagrams for fabrication of carbon nanotube membranes using nanotube array encapsulation with Si3N4 or polymers (A), and filtration-assisted alignment (B). (C-E) SEM images of (C) Si3N4-encapsulated membrane, from [39]; (D) Polystyrene encapsulated membrane, from [37]; and filtration-assisted assembly membrane, from [40]. © 2006, 2004 American Association for the Advancement of Science and 2001 American Chemical Society, respectively

4.1 Polymeric / CNT membranes. Hinds' group at the University of Kentucky has pioneered a membrane fabrication strategy based on polymer encapsulation of carbon nanotube arrays [37]. They infiltrated multi-wall CNT arrays with liquid polystyrene precursor that after curing produced a high density multiwall CNT membrane of ca. 7 nm pore size (Figure 3D). As the process occurs in the liquid phase, elaborate procedures were necessary to ensure that the CNTs do not bundle together upon solvent evaporation.

4.2 Silicon nitride CNT membranes. Our group developed a process for encapsulation of a vertically aligned array of carbon nanotubes with low-stress silicon nitride by a low pressure chemical vapor deposition process [38, 39]. This is a method widely used for a host of microfabrication processes and it produces an extremely conformal coatings around carbon nanotubes (Figure 3C). The membrane produced is robust and is capable of withstanding pressure gradients in excess of 1 atmosphere. Subsequent to encapsulation, the membrane undergoes a series of etching steps to selectively remove excess silicon nitride from the tips of the CNTs, followed by oxygen plasma to uncap the carbon nanotubes. Transmission electron micrographs of thinned-down sections of our double wall CNT (DWCNT) membranes (Figure 4) suggest that they consist of pores less than 2 nm diameter, consistent with diameters of as grown nanotubes, and no nano- or microvoids apparent in the structure. We have demonstrated fabrication of membranes with two different carbon nanotube pore diameters: double wall at 1.1nm <D<2nm and multi wall at ~6.5nm.

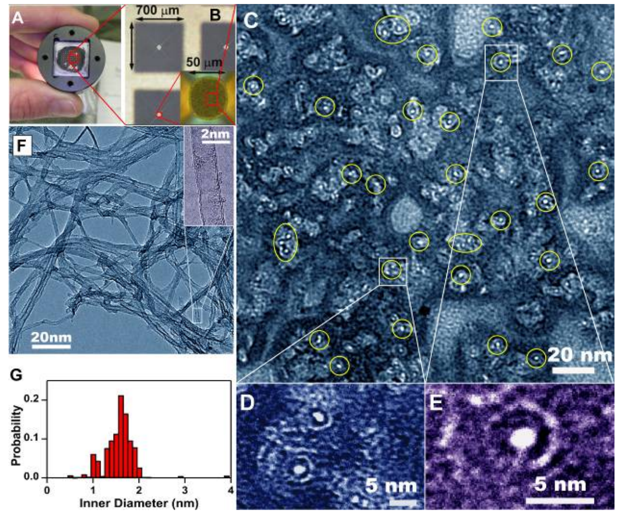

Figure 4. Sub-2-nm carbon nanotube membranes. (A) A photograph of a CNT membrane chip in the sample holder. (B,C) Optical micrographs of the regions of the chip that contain CNT membrane windows. (C-E) High-resolution TEM images of the thinned cross-sections of the membrane showing sub-2-nm pores. (F,G) HR-TEM characterization of the CNT size: (F) A TEM image of the dispersed carbon nanotubes from the vertically-aligned array used for membrane fabrication. (G) A histogram of measured inner diameters of carbon nanotubes. From [39] © 2006 American Association for the Advancement of Science

4.3 CNT polymer network fabrication. A considerably different approach to producing an aligned CNT – polymer composite membrane was recently described by E. Marand and co-workers (Figure 4B) [40]. Amine-functionalized CNTs were dispersed in tetrahydrofuran and subsequently filtered through a hydrophobic (0.2 micron) PTFE filter, leading to alignment within the membrane pores (Figure 3E). Spin coating with a dilute polymer solution (polysulfone) produced a mechanically stable thin film structure with the CNT tips protruding from the top of the membrane. Membranes produced with this method exhibited enhancements in gas transport rates and non-Knudsen selectivities for binary gas mixtures This approach has the advantage of being potentially more scalable and economical than direct growth CVD of CNTs on a substrate, although at the current stage of development the nanotube densities (and thus the available pore density) are much smaller than for the membranes produced by CNT array encapsulation.

5. Experimental observations of water transport in double-wall and multi-wall carbon nanotube membranes.

We also observed high rates of water transport through the double-wall sub-2-nm CNT membranes using pressure-driven flow [39]. Similarly high rates were also observed by Majumder et. al. for multiwalled nanotube membranes with larger pore diameters [41]. As previously discussed, the single largest uncertainty in quantifying the flux through individual pores lies in determination of the active pore density (i.e. those nanotubes which are open and span the membrane). Majumder et al. estimated the active pore densities by quantifying diffusion of small molecules through the CNTs. They measured enhancements of 4-5 orders of magnitude compared to Hagen-Poiseulle formalism. As described in the previous section, we estimated the upper bounds to the pore densities so that our measurements represent lower boundary estimates. The transport rates that we measured reveal a flow enhancement that is at least 2-3 orders of magnitude faster than no-slip, hydrodynamic flow calculated using Hagen-Poiseuille equation (Figure 5A). The calculated slip length for sub-2nm CNTs is as large as hundreds of nanometers, which is almost three orders of magnitude larger than the pore size and is almost on the order of the overall nanotube length. In contrast, the polycarbonate membrane with a pore size of 15 nm reveals a much smaller slip length of just 5 nm! This comparison suggests that slip flow formalism may not be applicable to water flow through carbon nanotubes, possibly due to length scale confinement [41, 42] or to partial wetting between water and the carbon nanotube surface [43].

Interestingly, the measured water flux compares well with that predicted by the MD simulations [29]. The simulations predict a flux of 12 water molecules per nm^2 (of nanotube cross sectional area) per ns; our measured flux, extrapolated to the simulation pressure drop, corresponds to 10-40 water molecules per nm^2 per ns [39]. Moreover, the measured absolute flow rates of at least 0.9 water molecule per nanotube is similar to the rate of 3.9 molecule/pore measured for aquaporins. The comparison to the aquaporins in not straightforward since the diameters of our CNTs are twice that of aquaporins and the CNTs are considerably longer, to name just a few differences. Therefore, we cannot yet imply that the same mechanism is responsible for transport in our CNTs and aquaporins. Nevertheless, our experiments demonstrate that the water transport through carbon nanotubes starts to approach the efficiency of biological channels.

6. Nanofiltration properties of carbon nanotube membranes

6.1 Size exclusion experiments in the 1-10nm size range.

Nearly frictionless graphitic walls of the CNT composite membranes offer the unique combination of extremely fast flow and very small pore size, which potentially give them a tremendous advantages over traditional membrane materials for energy-efficient, low-cost ultrafiltration and nanofiltration applications. Several experimental studies have used concentration gradient or pressure driven flow to determine the size exclusion properties of CNT composite membranes. Diffusion studies by Hinds' group showed that 10-nm gold nanoparticles were completely excluded by a multi-wall carbon nanotube (MWCNT)-membrane with pore inner diameter of ca. 7 nm, whereas small dyes (0.5-2 nm) diffuse with low hindrance [37, 41]. Our aligned DWCNT array membranes completely excluded 2-nm and 5-nm gold nanoparticles in pressure-driven filtration experiments as expected from the TEM measurements of the pore diameter (Figure 4F,G). Note that these membrane still exhibited extremely fast water permeation [39].

6.1 Ion exclusion in carbon nanotube membranes. With the diameters in the nm regime and high water permeabilities, carbon nanotubes are a promising platform for ion removal from water, as required for desalination and demineralization. MD simulations [44, 45] predict that if the nanotube is uncharged, size-based exclusion of small ionic species such as Na^+, K^+, or Cl^-, requires CNT diameters of about 0.4 nm. These diameters are comparable to the hydrated ion size. At this scale, the ion is forced to lose part of his hydration shell to enter the CNT, implying a very high energy barrier to cross the membrane (~ 120 KJ/mole). For slightly larger pore sizes (>1 nm), this free energy penalty decays almost to zero (~ 5 kJ/mole), allowing small ion free access. Molecular simulations [45] have also predicted that CNTs with 0.34-nm diameter, decorated with negative charges along the walls, conduct K^+ ions while excluding Cl^-, whereas positively charged CNTs with 0.47-nm diameter exclude K^+ ions while conducting Cl^-. Experimental verification of MD simulation prediction has not been achieved yet as CNT membranes with so small pore openings have not been successfully fabricated up-to-date. Joseph *et al.* showed by simulations that the presence of charged groups on the open CNT tips [46] induces preferential ion transport for carbon nanotube diameter of 2.2-nm. These results in particular suggest that dedicated functionalization of small-diameter CNT membranes (such as the membranes demonstrated by Holt et. al. [39]) may enable the control of ionic flow or even the exclusion of very small ions, a particularly exciting prospect for water purification and desalination.

Recently our team has performed the first evaluation of the ion exclusion in CNT membranes [47]. That study found that CNT membranes excluded a significant fraction of the ions in the feed solution (in some cases more than 90%). The exclusion characteristics of the membrane were also a strong function of the solution ionic strength with lower ionic strength exhibiting higher exclusion ratios. The last property provides a strong clue that electrostatic interactions on the CNT mouth play an important role. Further investigation showed that the rejection properties of the membrane obey the predictions of the Donnan equilibrium model. The exclusion properties observed for the CNT membrane are similar to the exclusion properties of the nanofiltration membranes with pores in the same size range. Notably CNT membranes are much thicker than the active layers of the nanofiltration membranes, yet they still exhibit much higher water flux!

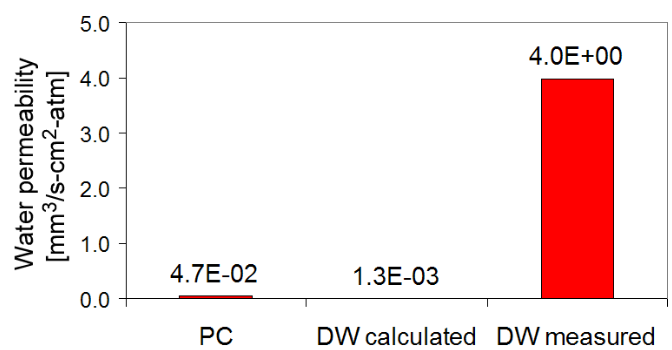

Figure 5. Water transport in sub-2-nm CNT membranes. Comparison of the water flux predicted for a polycarbonate membrane (left), and a double-wall carbon nanotube membrane (center) with the flux measured for the double-wall CNT membrane (right).

7. Altering transport selectivity by membrane functionalization.

An important avenue for controlling transport through the nanotube channels involves using chemical modifications of the nanotube to alter the channel permeability or exclusion characteristics. To maintain the efficient flow through the *nanotube* these treatments have to preserve the fundamental smoothness and hydrophobicity of the nanotube walls; therefore we will concentrate on the modification strategies that target only the entrance and the exit of the nanotube. In fact, most of the membrane fabrication strategies facilitate this approach by using an oxidation step to remove the fullerene cap from the nanotube. These procedures typically produces carboxylic groups at the mouth of the nanotube [48], which not only render the pore mouth negatively charged, but also could then serve as the target for a variety of chemical modification approaches [49, 50].

Most of the recent progress in this area has been associated with the works of Hinds and coworkers who used carbodiimide chemistry to attach a variety of organic and biological molecules to the mouth of carbon nanotubes. Interestingly, they observed that, for the polymer matrix based aligned nanotube membranes, the idealized picture of the oxidation step producing only a ring of carboxylic acid groups on the nanotube end and leaving the rest of the nanotube intact misrepresents the reality. Experiments on decorating the nanotube surface with gold nanoparticles showed that oxidation step produces reactive groups in the nanotube regions that are up to 700nm away from the tip of the nanotube [50, 51], although after only 50 nm of separation from the tip the functional group density was already significantly reduced. Researchers argue [50] that these apparent large penetration depths are consistent with the observation that the manufacturing process produces exposed carbon nanotube tips above the polystyrene matrix.

Majumder et. al. used carbodiimide chemistry to attach aliphatic chains, charged dye molecules, and polypeptides to the polystyrene-based carbon nanotubes membranes [50]. These modification has a measurable effect on the flux of the two large organic cations (methyl viologen (Mv^{2+}), and $Ru(bpy)_3^{2+}$) used for these experiments; for example, attaching a C_{40} alkane chain reduced the flux of Mv^{2+} by 6 times. Interestingly, the researchers did not observe a clear trend for the effect of the modification on the flux of the test species: for example, attaching a bulky charged organic dye to the mouth of the CNT membrane had actually increased the ion flux, presumably due to the interactions of the dyes molecules with the oppositely charged ions [50]. Also the relationship between the size of the modifier group and the effect on the charged species flux was complex; the authors of the report speculated that longer hydrophobic aliphatic chains prefer to orient along CNT walls and thus have a reduced effect on the overall flux.

8. Is energy-efficient desalination and water purification with carbon nanotube membranes possible and practical?

The definitive answer to this question will emerge only from continued research and development on the carbon nanotube membrane prototype. Yet, several conclusions can be reached even today. The most promising property of carbon nanotube membranes for water purification applications is their extremely high permeability. This property should translate into more water per unit of applied pressure, more efficient smaller purification units and ultimately into the lower purification or desalinations costs. Rich possibilities for chemical functionalization, coupled with the rather unique ability to manipulate only the chemistry at the nanotube mouth open up the possibility to production of membranes tailored for specific applications (for example RO desalination or impurity purification) while maintaining the basic membrane structure and high permeability.

However, a true assessment of the potential impact of the CNT membranes on the water purification (and specifically on water desalination) applications requires a more comprehensive comparison of the membrane characteristics with the general requirements of the membrane purification process. At least in the case of RO desalination, the process efficiency comes from three main sources: capital costs, energy costs, and operation costs (which include costs for pre-treatment, post-treatment and membrane cleaning and regeneration). It is instructive to evaluate the potential of the CNT membrane technology against these three areas. We first must note that the CNT technology is still in its infancy; therefore most attempts at quantitative evaluation will run up against large uncertainties associated with predicting the future technological milestones, or the fact that some of the major membrane characteristics (e.g. fouling properties) have not been sufficiently evaluated. Another large source of uncertainly is the lack of availability and cost estimate of a manufacturing process that allows scale-up of membrane fabrication.

However, we still can reach some qualitative conclusions based even on the limited set of data that is available now. The high flux of the CNT membranes provides a clear advantage for both the energy costs and the capital costs, as the same amount of water could be obtained with smaller driving pressures and less membrane area. However some of the other important advantages of the CNT membrane technology could come from the factors contributing the third cost factor: the operation costs. Uniform pore size of the CNT membranes could simplify or even eliminate the requirements for complicated multi-stage pretreatment efforts. The membrane pore surface is also rather chemically-inert, which could increase the membrane lifetime against the harsh agents used for pre treating water before RO or other purification steps. Unlike most polymeric membrane surfaces CNT membrane surface is hydrophilic; therefore it could offer an increased resistance to fouling, as well as easier cleanup by rinsing or backwashing. These factors all could contribute to an increased membrane lifespan and ultimately to operation cost savings.

If we consider these factors, it becomes clear that the real impact of the CNT membrane technology may lie in its potential to improve all of the major areas that contribute to the costs of water purification processes. Clearly, much work needs to be done before these promises translate into field applications. Researchers need to develop approaches for fabricating CNTs with even narrower distribution of the pore sizes, ideally with pores that are less than 1 nanometer. Targeted chemical modification of the pore entrances should improve dramatically the rejection characteristics of the membrane. Further studies are necessary to quantify the membrane fouling resistance and useful lifespan. Finally, development of large-scale, low-cost manufacturing processes is imperative to ensure that CNT membrane technology can achieve significant penetration into water purification market. These are all challenging tasks, yet the potential of the CNT membrane technology is high enough that we have no doubts that it will find its place in the arsenal of the water purification techniques available for mankind.

9. Acknowledgments

This chapter has been partially adapted from an invited review written by this team for the Nano Today magazine in 2007. C.G and O.B. acknowledge support from NSF NER 0608964; A.N., C.G., and O.B. acknowledge support from NSF NIRT CBET-0709090. All authors (except C.G.) acknowledge internal developmental funding support from LLNL. Parts of this work were performed under the auspices of the U.S. Department of Energy by Lawrence Livermore National Laboratory under Contract DE-AC52-07NA27344.

10. References.

1. Avlonitis, S.A., K. Kouroumbas, and N. Vlachakis, *Energy consumption and membrane replacement cost for seawater RO desalination plants.* Desalination, 2003. **157**(1-3): p. 151-158.
2. Spiegler, K.S. and Y.M. El-Sayed, *A Desalination Primer: Introductory Book for Students and Newcomers to Desalination*. 1994: Balaban Desalination Publications.
3. Shannon, M., et al., *Science and Technology for Water Purification in the Coming Decades.* Nature, 2008: p. accepted.
4. Terrones, M., *Science and technology of the twenty-first century: Synthesis, properties and applications of carbon nanotubes.* Ann. Rev. Mater. Res., 2003. **33**: p. 419-501.
5. Dresselhaus, M.S. and R. Saito, *Physical Properties of Carbon Nanotubes*. 1998: Imperial College Press.
6. Yamada, T., et al., *Size-selective growth of double-walled carbon nanotube forests from engineered iron catalysts.* Nature Nanotech., 2006. **1**(2): p. 131.
7. Futaba, D.N., et al., *Shape-engineerable and highly densely packed single-walled carbon nanotubes and their application as super-capacitor electrodes.* Nature Mater., 2006. **5**(12): p. 987-994.
8. Cheung, C.L., et al., *Diameter-controlled synthesis of carbon nanotubes.* J. Phys. Chem. B, 2002. **106**(10): p. 2429-2433.
9. Loiseau, A., et al., *Synthesis Methods and Growth Mechanics.* Lecture Notes in Physics, 2006. **677**: p. 49-130.

10. Franklin, N.R., et al., *Integration of suspended carbon nanotube arrays into electronic devices and electromechanical systems.* Appl. Phys. Lett., 2002. **81**(5): p. 913-915.
11. Puretzky, A.A., et al., *In situ measurements and modeling of carbon nanotube array growth kinetics during chemical vapor deposition.* Appl. Phys. A., 2005. **81**(2): p. 223-240.
12. Hummer, G., *Water, proton, and ion transport: from nanotubes to proteins.* Molecular Physics, 2007. **105**(2): p. 201 - 207.
13. Hummer, G., J.C. Rasaiah, and J.P. Noworyta, *Water conduction through the hydrophobic channel of a carbon nanotube.* Nature, 2001. **414**(6860): p. 188-190.
14. Kolesnikov, A.I., et al., *Anomalously Soft Dynamics of Water in a Nanotube: A Revelation of Nanoscale Confinement.* Phys. Rev. Lett., 2004. **93**(3): p. 35503.
15. Naguib, N., et al., *Observation of water confined in nanometer channels of closed carbon nanotubes.* Nano Lett., 2004. **4**(11): p. 2237–2243.
16. Maniwa, Y., et al., *Water-filled single-wall carbon nanotubes as molecular nanovalves.* Nature Materials, 2007. **6**(2): p. 135-141.
17. Mamontov, E., et al., *Dynamics of water confined in single-and double-wall carbon nanotubes.* J. Chem. Phys., 2006. **124**: p. 194703.
18. Waghe, A., J.C. Rasaiah, and G. Hummer, *Filling and emptying kinetics of carbon nanotubes in water.* J. Chem. Phys., 2002. **117**(23): p. 10789.
19. Beckstein, O., P.C. Biggin, and M.S.P. Sansom, *A Hydrophobic Gating Mechanism for Nanopores.* J. Phys. Chem. B, 2001. **105**(51): p. 12902-12905.
20. Beckstein, O. and M.S.P. Sansom, *Liquid-vapor oscillations of water in hydrophobic nanopores.* Proc. Natl. Acad. Sci. USA, 2003. **100**(12): p. 7063-7068.
21. Allen, R., S. Melchionna, and J.-P. Hansen, *Intermittent Permeation of Cylindrical Nanopores by Water.* Phys. Rev. Lett., 2002. **89**(17): p. 175502.
22. Allen, R., J.-P. Hansen, and S. Melchionna, *Molecular dynamics investigation of water permeation through nanopores.* J. Chem. Phys., 2003. **119**(7): p. 3905.
23. Andreev, S., D. Reichman, and G. Hummer, *Effect of flexibility on hydrophobic behavior of nanotube water channels.* J. Chem. Phys., 2005. **123**(19): p. 194502.
24. Wang, J., et al., *Diameter and helicity effects on static properties of water molecules confined in carbon nanotubes.* Phys. Chem. Chem. Phys., 2004. **6**(4): p. 829-835.
25. Won, C.Y., S. Joseph, and N.R. Aluru, *Effect of quantum partial charges on the structure and dynamics of water in single-walled carbon nanotubes.* J. Chem. Phys., 2006. **125**(11): p. 114701-9.
26. Huang, L.-L., et al., *Helicity and temperature effects on static properties of water molecules confined in modified carbon nanotubes.* Phys. Chem. Chem. Phys., 2006. **8**(33): p. 3836-3844.
27. Mashl, R.J., et al., *Anomalously Immobilized Water: A New Water Phase Induced by Confinement in Nanotubes.* Nano Lett., 2003. **3**(5): p. 589-592.
28. Won, C.Y. and N.R. Aluru, *Water Permeation through a Subnanometer Boron Nitride Nanotube.* J. Am. Chem. Soc., 2007. **129**(10): p. 2748-2749.
29. Kalra, A., S. Garde, and G. Hummer, *Osmotic water transport through carbon nanotube membranes.* Proc. Natl. Acad. Sci. USA, 2003. **100**(18): p. 10175-10180.
30. Sui, H., et al., *Structural basis of water-specific transport through the AQP1 water channel.* Nature, 2001. **414**(6866): p. 872-878.
31. Murata, K., et al., *Structural determinants of water permeation through aquaporin-1.* Nature, 2000. **407**(6804): p. 599-605.
32. Agre, P., et al., *Discovery of the aquaporins and their impact on basic and clinical physiology*, in *Aquaporins*. 2001. p. 1-38.
33. Kotsalis, E.M., J.H. Walther, and P. Koumoutsakos, *Multiphase water flow inside carbon nanotubes.* Int. J. Multiph. Flow, 2004. **39**: p. 995-1010.
34. Hanasaki, I. and A. Nakatani, *Flow structure of water in carbon nanotubes: Poiseuille type or plug-like?* J. Chem. Phys., 2006. **124**(14): p. 144708.
35. Striolo, A., *The Mechanism of Water Diffusion in Narrow Carbon Nanotubes.* Nano Lett., 2006. **6**(4): p. 633-639.
36. Che, G., et al., *Chemical vapor deposition based synthesis of carbon nanotubes and nanofibers using a template method.* Chem. Mater., 1998. **10**(1): p. 260-7.
37. Hinds, B.J., et al., *Aligned multiwalled carbon nanotube membranes.* Science, 2004. **303**(5654): p. 62-65.

38. Holt, J., et al., *Fabrication of a Carbon Nanotube-Embedded Silicon Nitride Membrane for Studies of Nanometer-Scale Mass Transport.* Nano Lett., 2004. **4**(11): p. 2245-2250.
39. Holt, J.K., et al., *Fast Mass Transport Through Sub-2-Nanometer Carbon Nanotubes.* Science, 2006. **312**(5776): p. 1034-1037.
40. Kim, S., et al., *Scalable Fabrication of Carbon Nanotube/Polymer Nanocomposite Membranes for High Flux Gas Transport.* Nano Lett., 2007. **7**(9): p. 2806 -2811.
41. Majumder, M., et al., *Nanoscale hydrodynamics: Enhanced flow in carbon nanotubes.* Nature, 2005. **438**(7064): p. 44-44.
42. Cottin-Bizonne, C., et al., *Nanorheology: An investigation of the boundary condition at hydrophobic and hydrophilic interfaces.* Europ. Phys. J. E., 2002. **9**(1): p. 47-53.
43. Craig, V.S.J., C. Neto, and D.R.M. Williams, *Shear-Dependent Boundary Slip in an Aqueous Newtonian Liquid.* Physical Review Letters, 2001. **87**(5): p. 54504.
44. Peter, C. and G. Hummer, *Ion transport through membrane-spanning nanopores studied by molecular dynamics simulations and continuum electrostatics calculations.* Biophys. J., 2005. **89**(4): p. 2222-2234.
45. Park, J.H., S.B. Sinnott, and N.R. Aluru, *Ion separation using a Y-junction carbon nanotube.* Nanotechnology, 2006. **17**(3): p. 895-900.
46. Joseph, S., et al., *Electrolytic transport in modified carbon nanotubes.* Nano Letters, 2003. **3**(10): p. 1399-1403.
47. Fornasiero, F., et al., *Ion Exclusion by sub 2-nm Carbon Nanotube Pores.* Proc. Natl. Acad. Sci. USA, 2007: p. submitted.
48. Hiura, H., T.W. Ebbesen, and K. Tanigaki, *Opening and purification of carbon nanotubes in high yields.* Adv. Mater., 1995. **7**(3): p. 275-276.
49. Wong, S.S., et al., *Covalently functionalized nanotubes as nanometrel-sized probes in chemistry and biology.* Nature, 1998. **394**(6688): p. 52-55.
50. Majumder, M., N. Chopra, and B.J. Hinds, *Effect of tip functionalization on transport through vertically oriented carbon nanotube membranes.* J. Am. Chem. Soc, 2005. **127**(25): p. 9062-9070.
51. Chopra, N., M. Majumder, and B. Hinds, *Bifunctional Carbon Nanotubes by Sidewall Protection.* Adv. Functl. Mater., 2005. **15**(5): p. 858-864.
52. Majumder, M., et al., *Voltage Gated Carbon Nanotube Membranes.* Langmuir, 2007. **23**(16): p. 8624-8631.

NANO LETTERS

2009
Vol. 9, No. 2
738-744

Mechanism and Kinetics of Growth Termination in Controlled Chemical Vapor Deposition Growth of Multiwall Carbon Nanotube Arrays

Michael Stadermann,[†] Sarah P. Sherlock,[†] Jung-Bin In,[†,§] Francesco Fornasiero,[†] Hyung Gyu Park,[†,‡,§] Alexander B. Artyukhin,[†] Yinmin Wang,[†] James J. De Yoreo,[‖] Costas P. Grigoropoulos,[§] Olgica Bakajin,[†,⊥] Alexander A. Chernov,[†] and Aleksandr Noy*,[†,#]

Physical and Life Sciences Directorate, Lawrence Livermore National Laboratory, Livermore, California 94550, Engineering Directorate, Lawrence Livermore National Laboratory, Livermore, California 94550, Department of Mechanical Engineering, University of California, Berkeley, Berkeley, California 94720, The Molecular Foundry, Lawrence Berkeley National Laboratory, Berkeley, California 94720, Center for Biophotonics Science and Technology, University of California, Davis, Sacramento, California 95616, and School of Natural Sciences, University of California, Merced, Merced, California 95344

Received October 30, 2008; Revised Manuscript Received November 26, 2008

ABSTRACT

We have investigated growth kinetics of multiwall carbon nanotube (MWCNT) arrays produced by catalytic thermal decomposition of ethylene gas in hydrogen, water, and argon mixture. The MWCNT growth rate exhibits a nonmonotonic dependence on total pressure and reaches a maximum at ~750 Torr of total pressure. Water concentrations in excess of 3000 ppm lead to the decrease in the observed growth rate. Optimal pressure and water concentration combination results in a reliable growth of well-aligned MWCNT arrays at a maximum growth rate of ~30 μm/min. These MWCNT arrays can reach heights of up to 1 mm with typical standard deviations for the array height of less than 8% over a large number of process runs spread over the time of 8 months. Nanotube growth rate in this optimal growth region remains essentially constant until growth reaches an abrupt and irreversible termination. We present a quantitative model that shows how accumulation of the amorphous carbon patches at the catalyst particle surface and the carbon diffusion to the growing nanotube perimeter causes this abrupt growth cessation. The influence of the partial pressures of ethylene and hydrogen on the ethylene decomposition driving force explains the nonlinear behavior of the growth rate as a function of total process pressure.

Vertically aligned carbon nanotube (CNT) arrays promise widespread use in a variety of applications ranging from field emission cathodes[1] and supercapacitors[2] to gas chromatography columns[3] and nanoelectronic devices, to sensors[4] and nanofiltration membranes.[5,6] Catalytic CVD growth, in which a mixture of the carbon feedstock gases flows over the metal nanoparticle catalyst at high temperatures,[7] readily produces such arrays in laboratory conditions.[1] However, growth mechanisms and, in particular growth termination mechanisms, are still poorly understood.[4,8] As the result, synthetic control over nanotube diameter, chirality, and length is either limited or nonexistent.

Researchers have reported numerous process parameters such as feed gas mixture composition and flow rate, growth temperature, reaction pressure, catalyst composition, and annealing conditions[7,9−13] that can dramatically change the yield of the nanotube arrays and quality of the carbon nanotubes. Despite these studies, in many instances it is still difficult to achieve reproducible nanotube array growth even when using identical process parameters. These problems can partially explain limited use of aligned CNT arrays in real-world applications as well as point to the reason why only a few kinetic studies of nanotube growth exist to date.[8,14,15]

* Corresponding author, noy1@llnl.gov.
† Physical and Life Sciences Directorate, Lawrence Livermore National Laboratory.
‡ Engineering Directorate, Lawrence Livermore National Laboratory.
§ Department of Mechanical Engineering, University of California, Berkeley.
‖ The Molecular Foundry, Lawrence Berkeley National Laboratory.
⊥ Center for Biophotonics Science and Technology, University of California, Davis.
School of Natural Sciences, University of California, Merced.

10.1021/nl803277g CCC: $40.75
Published on Web 01/15/2009

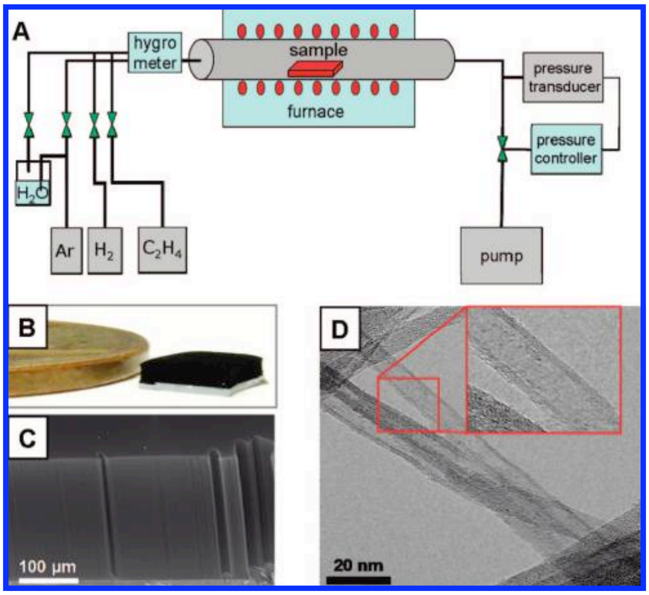

Figure 1. Carbon nanotube array growth and characterization. (A) Schematic of the CVD growth setup. Mass flow controllers set the flow of all process gases to the system. A hygrometer controls the water content of the gas mixture before it enters the furnace, and the pressure at which the reaction takes place is controlled at the exhaust end. (B) A photograph showing a tall MWNT film on a silicon substrate next to a penny coin. (C) SEM image of the nanotube mat grown at 750 °C, 760 Torr, 2000 ppm of water for 10 min. (D) TEM image of the MWNTs grown at the same conditions as the array in (B).

In this work we investigated the growth efficiency and growth kinetics for vertically aligned CNT array growth on silicon substrates. We present the data that show that variations in growth conditions have a substantial effect on the CNT array growth rates. We then discuss the mechanistic basis for the observed effects and propose a model that reproduces most of the features of the observed growth kinetics.

Materials and Methods. Carbon nanotube growth experiments were performed in a 1 in. tube furnace (Lindberg Blue TF55035A) modified for control over the process pressure and water content of the feed gas (Figure 1A). All of our studies were performed using ethylene as our carbon source. The feed gas mixture always had 30% argon, 20% hydrogen, and 50% ethylene, while total flow rates varied from 100 to 2000 sccm. To add water to the gas mixture, we split the argon line into two streams, pass one of the streams through a water bubbler, and then adjust the splitting ratio so that mixing wet argon and dry argon produces the desired humidity while retaining a total argon fraction of 30%. The water content of the feed gas was measured with a hygrometer at the furnace entrance. We find that the hygrometer is essential for obtaining reproducible water concentrations; simply controlling the temperature of the bubbler and mixing the same amount of wet argon to the gas mixture does not yield reproducible water concentrations due to a gradual drying of the gas lines. Our system uses two hygrometers, a Nyad Inc. model 160 and a Bartec Hygrophil F5672. The first hygrometer equilibrates much faster than the other one but is prone to decalibrating over time. The Hygrophil F5672 gives consistent readings but takes a relatively long time to equilibrate. By using the "slow" hygrometer to provide a reference for the "fast" hygrometer, we can control the humidity in real time while still having an accurate overall humidity value. We controlled the process pressure with a custom-built feedback system consisting of manometer, control valve, and pressure controller placed at the exhaust end of the furnace (calculated error in the pressure determination due to the hydrodynamic resistance of the piping between the manometer and the reaction chamber is less than 0.01%). This system holds constant pressure to within 0.2 Torr accuracy, over the 100−1000 Torr range.

Our nanotube growth catalyst consists of 10 nm Al and 3 nm Fe films deposited onto the surface of a Si wafer with native oxide by e-beam evaporation. Before growth, the samples were oxidized in air at 500 °C for 15 min. Then the temperature was ramped up at 40 °C/min to 750 °C while flowing argon and hydrogen and held at 750 °C for 12 min before adding ethylene. The water is adjusted after the sample annealed for 2 min at 750 °C. The growth was timed from the moment the mass flow controller was opened. We measured the height of the tall forests (higher than 60 μm) with an optical microscope; shorter arrays were characterized by imaging the array cross section with a Hitachi S-800 scanning electron microscope.

Raman spectra were collected with Nicolet Almega XR dispersive micro-Raman spectrometer using 473 and 633 nm excitation length and 100× collection objective. Scanning electron microscopy (SEM) images were obtained using JEOL 7401F and Hitachi S800 scanning electron microscopes. Transmission electron microscopy (TEM) images were recorded on a Philips CM300-FEG TEM operated at 300 kV and equipped with a Gatan image filter system. The extraction voltage for the field-emission gun was 4.2 keV. The spatial resolution of the microscope is approximately 1.8 Å.

CNT Array Growth Yield. When we performed systematic variation of total gas pressure and water concentration in our chemical vapor deposition (CVD) system (Figure 1A), we found that they resulted in the large variations in the height of the CNT arrays produced after 10 min of growth. This height value reaches a maximum as functions of the total pressure at ~700 Torr. Water concentration above ~2500 ppm diminishes the growth rate. Remarkably, we found a very stable region around 760 Torr of total process pressure and 1500 ppm H_2O content that maximizes the CNT growth rate (Figure 2) and routinely and reproducibly produces carbon nanotube arrays (Figure 1B,C) of up to 1 mm in height. The water/ethylene ratio in this region is 1/330, which curiously is within a factor of 3 of the optimal water/ethylene ratio previously reported by Futaba et al. for growth of single-wall carbon nanotube (SWNT) arrays.[14] Qualitatively, the observed sensitivity of the CNT growth to the feed gas pressure and water concentration is not surprising, since the total pressure affects the partial pressures of the reaction species and, thus, ultimately determines the incoming flux of carbon to the catalyst. The primary role of the water is assumed to oxidize and remove amorphous carbon

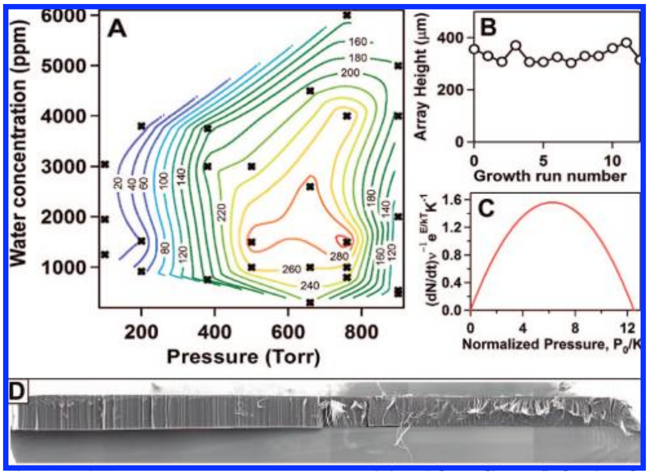

Figure 2. CVD process parameter space. (A) A "phase diagram" showing the nanotube array height measured after 10 min of growth as a function of water concentration and total process pressure. All growth runs were performed at 750 °C. The crosses mark the points in the parameter space where measurements were performed. The topographical lines are extrapolated and serve to guide the eye. The numbers on the topographical lines are array heights in micrometers. (B) Plot of measured CNT array height obtained in 13 growth runs using identical growth parameters and spaced over an 8 month period. (C) Plot of the predicted normalized rate of pyrolyzed carbon (CNT growth precursor) production predicted by eq 10 as a function of the normalized total process pressure. (D) SEM micrograph of a cross section of ~350 μm tall CNT array on the Si substrate demonstrating growth uniformity over large scale.

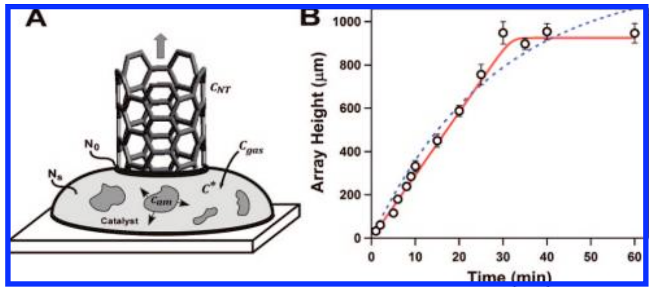

Figure 3. Mechanism and kinetics of growth termination. (A) Schematics of the poisoning/diffusion model of carbon nanotube growth termination. Growth proceeds through a two-stage process that involves conversion of the gas-phase precursor C_{gas} to an activated surface-bound form, C*. C* can then diffuse through the catalyst particle and incorporate into a growing nanotube, or form amorphous carbon patches C_{am} that block the catalyst particle surface. The figure also indicates various concentration of the carbon atoms used in the model description. Note that the catalyst particle shown in this figure is used as only as a simplified representation and does not reflect the true geometry of the catalyst/CNT system. (B) Plot of the measured nanotube array height (open circles) as a function of the growth time. Each data point represents an average of at least three individual growth runs. The red solid line corresponds to the best fit to eqs 6 and 7 using the calculated value of $G_D = 2.2 \times 10^5$ μm/min; the parameters producing the best fit were $G_0 = 30.7$ μm/min, $\tau = 14.5$ min. The dotted blue line is the best fit to the data using the exponential growth model by Iijima and co-workers.[14]

on the catalyst, along with etching the graphitic carbon, which could also have drastic effects on the CNT growth.[16]

The height of the CNT arrays grown at the optimal conditions in our system was extremely uniform and varied by only 1−2% over the sample (Figures 1C and 2D). The data were highly reproducible from run to run: nanotube array height measured after 13 different 10 min long growth runs over the course of 8 months using three different catalyst depositions showed standard deviation of only 7.8% (Figure 2B). The TEM analysis indicates that growth in the optimal region of the parameter space produces multiwall carbon nanotubes (MWNTs) with well-graphitized sidewalls and low concentration of defects (Figure 1D).

Outside the optimal growth plateau region the growth rate drops quickly (Figure 2A). In general, the growth rate shows a stronger dependence on pressure than on water content, especially in the high pressure region; although water content variations alone could produce up to 50% difference in growth height. The strong growth rate dependence on pressure, away from the dome top in Figure 2A, suggests that even day-to-day atmospheric pressure fluctuations can lead to significant height changes. This observation might explain why some recipes found in literature for growth at ambient pressures yield inconsistent results.

CNT Arrays Growth Kinetics. To gain insight into the microscopic mechanism of the CVD growth at the optimal conditions, we have studied growth kinetics by terminating the reaction at different growth times. Since our growth was very reproducible from run to run, this method allowed us to obtain a highly accurate kinetic curve (Figure 3B). Our data show that growth of MWNT in the optimal regime does not follow an exponential growth kinetics reported in several other studies.[8,14] Instead, the growth proceeds at constant rate, where the array height increases linearly with time, and then abruptly terminates as the array reaches its maximum height value. A similar abrupt termination kinetics was also reported recently by other research groups.[15,17] All of our growth runs indicate that the catalyst remains on the bottom of the sample during the growth process. Indeed, the backscatter-electron imaging with SEM showed no metal particles at the top of the array and the catalyst particles were found remaining at the substrate after mechanical removal of the nanotube array. If the growth process was terminated before the system entered the growth height plateau region, the nanotube growth could be restarted, albeit at an overall reduced rate (see Figure S3 in Supporting Information). In contrast, once the growth stopped it could not be resumed. Clearly, these data contradict the commonly used exponential growth decay model that assumes monotonic decrease in catalyst activity over time.[14] We have also noticed significant edge effects (i.e., array edges being higher or lower than the center region) for the arrays grown at nonoptimal conditions (see Figure S1a,b, Supporting Information). Curiously, these effects are virtually absent for the arrays grown at the optimal conditions where we observed extremely uniform edge-to-edge array thickness (Figure 2c).

CNT Growth Cessation. The growth cessation may be caused either by poisoning of the catalyst, or of the carbon nanotube's growth front, or by limitations imposed by diffusion of carbon feedstock to the catalyst surface through the dense array of CNTs. Maruyama and co-workers recently analyzed the feedstock diffusion limitations in the CNT growth process[18] and found that for MWNT growth the diffusion does not limit the growth kinetics until the arrays grow to the lengths that are more than an order of magnitude higher than arrays obtained in our study. Also, the growth rate limited by gas diffusion to/from the catalyst particle down through the CNT array of height H_g should decrease as $1/H_g$, i.e., much more gradually than that observed in our experiments. High-resolution SEM images show that before the growth cessation, nanotubes emerging from Fe catalyst particles lose their general alignment and become randomly oriented over several micrometers near the substrate (Figure S2 in the Supporting Information). This behavior suggests a spatial growth instability that hardly could be ascribed to poisoning of the perimeter of the growing nanotube, since poisoning particles are usually irreversibly attached to the interface that they poison;[19] therefore poisoning of the growing end of a nanotube is also unlikely.

Thus, we conclude that the catalyst poisoning is the most probable cause for the growth cessation. Most likely the poisoning species is amorphous carbon. First, the presence of water vapor that etches amorphous carbon leads to an substantial enhancement of the nanotube growth yield.[20] Second, micro-Raman spectroscopy mapping (see Figure S1 in the Supporting Information) revealed that the G/D band intensity ratio has continuously decreased during the array growth, indicating increasing concentration of amorphous carbon near the catalyst surface species at the end of the growth process (G-band Raman signal typically indicates the level of graphitized carbon, while D-band corresponds to disordered amorphous carbon).

What is the mechanism of the growth poisoning? We first describe a qualitative model that accounts for the kinetic features observed in our growth experiments. We postulate that carbon nanotube growth proceeds in two stages. At first the ethylene molecule adsorbs on the surface of the catalyst particle and is ultimately converted into a carbon atom C, which can diffuse to the catalyst particle step edge and incorporate into a nanotube.[21,22] Alternatively, it may nucleate a new amorphous carbon cluster or join an already existing one (Figure 3A). These cluster patches eventually grow to cover the surface of the catalyst particle thus blocking the ethylene decomposition and carbon supply to the nanotube. This mechanism explains irreversible growth cessation. Indeed, Ajayan and co-workers reported that after the 10 min of high-temperature oxidation, the catalyst activity resumes, and a second nanotube array may be grown on the same substrate, while further oxidation may detach the array sandwich from the substrate. Probably, this harsh oxidation removes the amorphous carbon film along with the curved defect-rich nanotube portions, and reactivates the catalyst.[23] Additionally, we expect that when the carbon patches cover the catalyst particle surface almost completely, the feeding of the growing nanotube perimeter becomes spatially asymmetric and varying in time. That asymmetry changes the tube orientation and induces the increased entanglement observed in the last stages of the array growth (Figure S2, Supporting Information).

We now use this model to construct a semiquantitative description of the growth and poisoning kinetics. According to the classical Kolmogorov−Johnson−Mehl−Avrami (KJMA) theory,[19,24−26] the fraction, $g(t)$, of the surface not yet covered by the passivating patches by the time t after the start of the deposition is given by

$$g(t) = \exp\left[-\frac{\pi J V^2 t^3}{3}\right] \tag{1}$$

The KJMA theory is strictly applicable if the total size of the system is much larger than the distance between the (round) patches, and a more exact description would include a correction for the finite size of the surface. Our derivation is based on a simple KJMA model (eq 1), and therefore it should be considered as an approximation. The overall carbon nanotube growth rate υ_g would be proportional to the open surface area of the catalyst

$$\upsilon_g = \upsilon_0 g(t) = \upsilon_0 \exp\left[-\frac{\pi J V^2 t^3}{3}\right] \tag{2}$$

where J (1/(m^2 s)) is the rate of the amorphous carbon nucleation, V (m/s) is the linear expansion rate of a patch, and υ_0 (m/s) is the nanotube growth rate on a clean catalyst. The parameter υ_0 is controlled by the delivery of the carbon atoms to the growing nanotube perimeter and incorporation rate, and we can estimate it using the model of Tibbetts et al.[27] Briefly, this model postulates that carbon species adsorb from the gas phase onto the surface of the catalyst particle and creates a carbon concentration on the surface that is highly supersaturated with respect to the carbon concentration at the perimeter of the growing carbon nanotube. Concentration gradient then leads the carbon atoms to diffuse through the iron particle and incorporate into the nanotube. Although the real geometry of the catalyst particle and a growing carbon nanotubes is complicated, we follow Tibbetts and co-workers by modeling the catalyst particle as a cylinder of radius and thickness equal to the outer radius of the carbon nanotube R_0. Under these assumptions, the growth rate υ_g is

$$\upsilon_g = \frac{J_s \Omega}{1 - \left(\frac{r_i}{r_o}\right)^2} \frac{N_s - N_0}{N_s} \frac{1}{1 + \frac{J_s R}{D N_s}} \tag{3}$$

Here J_s (1/(m^2 s)) is the effective incoming flux of carbon atoms that accounts for ethylene adsorption, its thermal decomposition that produces carbon on the catalyst−gas interface, and hydrogen release back to the gas phase, along with inverse reactions that produce volatile hydrocarbons from adsorbed C and gaseous hydrogen. Finally, J_s includes an energy barrier that C atoms must overcome to dissolve in the solid Fe−C catalyst (likely austenite). N_s (1/m^3) is the bulk concentration of mobile carbon atoms in the catalyst just below its interface, and N_0 is the carbon atom concentration in equilibrium with the perimeter of the growing carbon nanotube (this concentration could also include contributions from carbon atoms delivered by surface diffusion). The $2r_o$ and $2r_i$ are the outer and inner diameters of the carbon nanotube, D is the effective diffusivity of carbon atoms that accounts for both bulk and surface diffusion over the effective distance R of the order of the catalyst radius, and Ω is the volume of a carbon atom in graphite.

The ratio J_sR/DN_s defines the ratio of the carbon production rate J_s to the carbon diffusion rate. Precipitation of amorphous carbon observed in the Raman spectroscopy data, along with nanotube graphite, suggests that supersaturation of carbon in the catalyst particle and on the catalyst surface is high enough to drive the growth process. Therefore, it is reasonable to assume that $N_s \gg N_0$. That assumption simplifies eq 3 to:

$$v_g = \frac{J_s\Omega}{1-\left(\frac{r_i}{r_o}\right)^2}\frac{1}{1+\frac{J_sR}{DN_s}} \tag{4}$$

The impact of amorphous carbon patches formation manifests itself as the reduction of the catalyst surface area where the carbon is produced from ethylene while the concentration of carbon on the still poison-free surface does not change. Then, the *average* carbon concentration over the whole catalyst interface will be

$$N_s(t) = N_s^{\ 0}g(t) = N_s^{\ 0}\exp\left[-\frac{t^3}{\tau^3}\right] \tag{5}$$

where N_s^o is the carbon concentration on a clean catalyst particle and τ is the characteristic poisoning time $\tau = (3/\pi JV^2)^{1/3}$. We now can combine eqs 2, 4, and 5 into a simple expression

$$v_g = \frac{G_0}{1+\frac{G_0}{G_D}\exp\left[\frac{t^3}{\tau^3}\right]} \tag{6}$$

where

$$G_0 = \frac{J_s\Omega}{1-(r_i/r_o)^2}$$

and

$$G_D = \frac{D\Omega N_s^{\ 0}}{R[1-(r_i/r_o)^2]}$$

Finally, the observed height H_g of the carbon nanotube array is

$$H_g = \int_0^t v_g(t)\,dt \tag{7}$$

Equation 6 contains three parameters: characteristic poisoning time, τ, the growth rate G_0 on the clean catalyst at the infinitely fast diffusion, and the growth rate G_D, also on a clean catalyst, but fully controlled by slow diffusion (i.e., growth rate at an infinitely fast supply of carbon). Note that at least initially the diffusion through the catalyst particle should not limit the growth speed, i.e., $G_D \gg G_0$.

We can estimate G_D by assuming that we can approximate the value of N_s by the volumetric concentration of carbon atoms in a graphite layer (37.9 atoms/nm^{-3}) and by using the literature values for the diffusion coefficient of carbon in iron at 1023 K (750 °C), $D = 3.2 \times 10^{-7}$ cm^2/s, volume of carbon atom $\Omega = 8.8 \times 10^{-3}$ nm^3, and the value of r_o = 3.1 nm from the TEM measurements. Under these assumptions we calculate the value of $G_D = 2.2 \times 10^5$ μm/min.

We can also estimate the parameter G_D using a slightly different argument. The atomic fraction of carbon in iron at equilibrium with graphite (and MWCNT), ΩN_0, could hardly exceed the maximum atomic fraction of C in austenite (~7 $\times 10^{-2}$ at 1100 K). The equivalent fraction of carbon in a highly supersaturated solution, ΩN_0, should be noticeably higher. If we assume a supersaturation of 10 ($(N_s - N_0)/N_0 = 10$), and use the calculated carbon diffusivity in the BCC iron of 1.8×10^{-7} cm^2/s at 1100 K[28] (which is not far away from the value $D = 3.2 \times 10^{-7}$ cm^2/s used for the previous estimate) and the catalyst radius $R = 3.1$ nm, then we arrive at the estimate of $G_D = 2.4 \times 10^5$ μm/min, which is quite close to the value obtained from the previous estimate.

Best fits of eqs 6 and 7 to our kinetic data (Figure 3B) using the calculated value of $G_D = 2.2 \times 10^5$ μm/min show that our model reproduces the key feature of the growth process—the nearly constant array growth rate followed by an abrupt growth termination—over the whole range of the growth times. The value of the parameter obtained from the fit, $G_0 = 30.7$ μm/min, is indeed much smaller than the value of G_D, thus providing another consistency check for our model. Finally, we note that the exponential growth rate decay (dotted line in Figure 3B) does not describe the abrupt growth cessation observed in the experiment.

Growth Rate and the Total Process Pressure. The observed nonlinear dependence of the measured growth rate as a function of the total pressure (Figure 2A) could be rationalized by considering the ethylene/hydrogen balance in overall thermal decomposition reaction

$$C_2H_4 \leftrightarrow 2H_2 + 2C$$

At equilibrium, this reaction is described by the following balance of chemical potentials

$$\mu_{C_2H_4} = 2\mu_{H_2} + 2\mu_C \tag{8}$$

or

$$k_BT\ln\frac{P_{C_2H_4}}{P_{H_2}^{\ 2}} = K = 2\mu_C + 2\mu_{H_2}^{\ 0} - \mu_{C_2H_4}^{\ 0}$$

were the subscripts denote the chemical species, μ^o_i is the standard state chemical potential of the species $i$and K is the equilibrium constant. Away from equilibrium, the net carbon production per unit time per unit catalyst area, i.e., $2J_s$, is given by the difference between rate of the C_2H_4 decomposition and the reverse reaction rate. The decomposition occurs when an adsorbed C_2H_4 molecule overcomes the activation barrier E_a for decomposition; hence the chance to find the ethylene molecule in this exited state is $e^{(\mu(C_2H_4)-E_a)/kT}$. Similarly, the probability of the inverse reaction is given by $e^{(2\mu(C)+2\mu(H_2)-E_a)/kT}$. Since ethylene decomposition requires dissociation of a covalent bond, it is reasonable to expect that the activation energy for this process will be much higher than the adsorption energies for C_2H_4 and H_2; therefore it is reasonable to assume that the adsorbed ethylene and hydrogen molecules are in equilibrium with the gas phase and that the corresponding chemical potentials, $\mu_{C_2H_4}$ and μ_{H_2} are equal in the adsorbed and gaseous states. If the deviations from the equilibrium are not extreme, the pre-exponent frequency factors, ν, for the direct and inverse reactions should be equal. Therefore the carbon production flux may be approximated as

$$2J_s = \nu e^{(\mu(C_2H_4)-E_a)/k_BT} - \nu e^{(2\mu(H_2)+2\mu(C)-E_a)/k_BT} = \nu e^{-E_a/k_BT}(e^{(\mu(C_2H_4)-2\mu(H_2)-2\mu(C))/k_BT} - 1)e^{(2\mu(H_2)+2\mu(C))/k_BT} \quad (9)$$

Finally, we can rewrite this equation as:

$$v_g \sim \nu e^{-E_a/k_BT} K P_{H_2}{}^2 \left(\frac{P_{C_2H_4}}{P_{H_2}{}^2 K} - 1 \right) = \nu e^{-E_a/k_BT}(\xi_{C_2H_4} P_0 - K\xi_{H_2}^2 P_0{}^2) \quad (10)$$

where the constants ξ_i denotes the volume fractions of a particular gas in the gas mixture. It is clear from the last two terms of the eq 10 that as the total pressure P_0 increases, the carbon production at first rises but then starts to decrease as the quadratic term starts to overwhelm the linear term. In other words, carbon production always increases proportionally to P_0, while carbon removal by hydrogen increases as $P_0{}^2$. The data do show a very similar trend with the variations of process pressure (Figure 2A). Finally, the observed decrease in the CNT growth rates with the increase of water concentration likely reflects the etching of both the amorphous carbon and the graphitic carbon. The presence of significant amounts of water in the reaction mixture introduces a more complicated set of reaction processes that our model does not capture at this point.

Reproducible growth of nanotube arrays under controlled conditions that we have demonstrated removes many obstacles to the technological applications of carbon nanotube arrays. Tight control over CNT array dimensions should enable their incorporation into the MEMS and NEMS devices using processes and architectures that require high reproducibility and close matching of the components. We also showed that the kinetics of CNT array growth can be described quantitatively using a simple model that considers carbon pyrolysis equilibrium, carbon diffusion through the catalyst particle, and poisoning of the catalyst surface. Further refinements to this model should lead to a better understanding and better control of CNT growth by thermal CVD.

Acknowledgment. S.S. acknowledges support from the USI program at LLNL, A.A. and H.G.P. acknowledge support from the LLNL SEGRF fellowship program. This work was partially supported by the DARPA MGA program, Office of Basic Energy Science (BES) Division of Materials Science and Engineering, CA State DWR grant, and the NSF NIRT Grant CBET-0709090. Parts of this work were performed under the auspices of the U.S. Department of Energy by Lawrence Livermore National Laboratory under Contract DE-AC52-07NA27344.

Supporting Information Available: Figures showing micro-Raman spectroscopy of the VA-CNT array and termination of growth, both macroscopic and microscopic behavior. This material is available free of charge via the Internet at http://pubs.acs.org.

References

(1) Fan, S. S.; Chapline, M. G.; Franklin, N. R.; Tombler, T. W.; Cassell, A. M.; Dai, H. J. Self-oriented regular arrays of carbon nanotubes and their field emission properties. *Science* **1999**, *283* (5401), 512–514.

(2) Niu, C. M.; Sichel, E. K.; Hoch, R.; Moy, D.; Tennent, H. High power electrochemical capacitors based on carbon nanotube electrodes. *Appl. Phys. Lett.* **1997**, *70* (11), 1480–1482.

(3) Saridara, C.; Mitra, S. Chromatography on self-assembled carbon nanotubes. *Anal. Chem.* **2005**, *77* (21), 7094–7097.

(4) Dai, H. J. Carbon nanotubes: synthesis, integration, and properties. *Acc. Chem. Res.* **2002**, *35* (12), 1035–1044.

(5) Holt, J. K.; Park, H. G.; Wang, Y.; Stadermann, M.; Artyukhin, A. B.; Grigoropoulos, C. P.; Noy, A.; Bakajin, O. Fast mass transport through sub-2-nanometer carbon nanotubes. *Science* **2006**, *312* (5776), 1034–1037.

(6) Hinds, B. J.; Chopra, N.; Rantell, T.; Andrews, R.; Gavalas, V.; Bachas, L. G. Aligned multiwalled carbon nanotube membranes. *Science* **2004**, *303* (5654), 62–65.

(7) Hafner, J. H.; Bronikowski, M. J.; Azamian, B. R.; Nikolaev, P.; Rinzler, A. G.; Colbert, D. T.; Smith, K. A.; Smalley, R. E. Catalytic growth of single-wall carbon nanotubes from metal particles. *Chem. Phys. Lett.* **1998**, *296* (1−2), 195–202.

(8) Puretzky, A. A.; Geohegan, D. B.; Jesse, S.; Ivanov, I. N.; Eres, G. In situ measurements and modeling of carbon nanotube array growth kinetics during chemical vapor deposition. *Appl. Phys. A: Mater. Sci. Process.* **2005**, *81* (2), 223–240.

(9) Christen, H. M.; Puretzky, A. A.; Cui, H.; Belay, K.; Fleming, P. H.; Geohegan, D. B.; Lowndes, D. H. Rapid growth of long, vertically aligned carbon nanotubes through efficient catalyst optimization using metal film gradients. *Nano Lett.* **2004**, *4* (10), 1939–1942.

(10) Kong, J.; Soh, H. T.; Cassell, A. M.; Quate, C. F.; Dai, H. J. Synthesis of individual single-walled carbon nanotubes on patterned silicon wafers. *Nature* **1998**, *395* (6705), 878–881.

(11) Delzeit, L.; Chen, B.; Cassell, A.; Stevens, R.; Nguyen, C.; Meyyappan, M. Multilayered metal catalysts for controlling the density of single-walled carbon nanotube growth. *Chem. Phys. Lett.* **2001**, *348* (5−6), 368–374.

(12) Su, M.; Zheng, B.; Liu, J. A scalable CVD method for the synthesis of single-walled carbon nanotubes with high catalyst productivity. *Chem. Phys. Lett.* **2000**, *322* (5), 321–326.

(13) Ci, L. J.; Xie, S. S.; Tang, D. S.; Yan, X. Q.; Li, Y. B.; Liu, Z. Q.; Zou, X. P.; Zhou, W. Y.; Wang, G. Controllable growth of single wall carbon nanotubes by pyrolizing acetylene on the floating iron catalysts. *Chem. Phys. Lett.* **2001**, *349* (3−4), 191–195.

(14) Futaba, D. N.; Hata, K.; Yamada, T.; Mizuno, K.; Yumura, M.; Iijima, S. Kinetics of water-assisted single-walled carbon nanotube synthesis revealed by a time-evolution analysis. *Phys. Rev. Lett.* **2005**, *95* (5), 056104−4.

(15) Meshot, E. R.; Hart, A. J. Abrupt self-termination of vertically aligned carbon nanotube growth. *Appl. Phys. Lett.* **2008**, *92*, 113107.

(16) Hata, K.; Futaba, D. N.; Mizuno, K.; Namai, T.; Yumura, M.; Iijima, S. Water-assisted highly efficient synthesis of impurity-free single-waited carbon nanotubes. *Science* **2004**, *306* (5700), 1362–1364.

(17) Puretzky, A. A.; Eres, G.; Rouleau, C. M.; Ivanov, I. N.; Geohegan, D. B. Real-time imaging of vertically aligned carbon nanotube array growth kinetics. *Nanotechnology* **2008**, *19* (5), 55605.

(18) Xiang, R.; Yang, Z.; Zhang, Q.; Luo, G.; Qian, W.; Wei, F.; Kadowaki, M.; Einarsson, E.; Maruyama, S. Growth deceleration of vertically aligned carbon nanotube arrays: catalyst deactivation or feedstock diffusion controlled. *J. Phys. Chem. C* **2008**, *112* (13), 4892–4896.

(19) Chernov, A. *Modern crystallography v.III: Crystal growth* Springer-Verlag: Berlin and New York, 1984; Vol. 36, p 517.

(20) Hata, K.; Futaba, D. N.; Mizuno, K.; Namai, T.; Yumura, M.; Iijima, S. Water-assisted highly efficient synthesis of impurity-free single-walled carbon nanotubes. *Science* **2004**, *306* (5700), 1362–1364.

(21) Helveg, S.; Lopez-Cartes, C.; Sehested, J.; Hansen, P. L.; Clausen, B. S.; Rostrup-Nielsen, J. R.; Abild-Pedersen, F.; Noerskov, J. K. Atomic-scale imaging of carbon nanofibre growth. *Nature* **2004**, *427* (6973), 426–429.

(22) Abild-Pedersen, F.; Norskov, J. K.; Rostrup-Nielsen, J. R.; Sehested, J.; Helveg, S. Mechanisms for catalytic carbon nanofiber growth studied by ab initio density functional theory calculations. *Phys. Rev. B* **2006**, *73* (11), 115419−13.

(23) Ci, L. J.; Manikoth, S. M.; Li, X. S.; Vajtai, R.; Ajayan, P. M. Ultrathick freestanding aligned carbon nanotube films. *Adv. Mater.* **2007**, *19* (20), 3300–3300.

(24) Johnson, W.; Mehl, R. Reaction kinetics in processes of nucleation and growth. *Trans. Am. Inst. Min., Metall. Pet. Eng.* **1939**, *135*, 416.
(25) Kolmogorov, A. On statistical theory of metal crystallisation. *Izv. Akad. Nauk SSSR, Ser. Mat.* **1937**, *3*, 355.
(26) Avrami, M. Granulation, phase change, and microstructure kinetics of phase change. III. *J. Chem. Phys.* **1941**, *9* (2), 177–184.
(27) Tibbetts, G. G.; Devour, M. G.; Rodda, E. J. An adsorption-diffusion isotherm and its application to the growth of carbon filaments on iron catalyst particles. *Carbon* **1987**, *25* (3), 367–375.
(28) Jiang, D. E.; Carter, E. A. Carbon dissolution and diffusion in ferrite and austenite from first principles. *Phys. Rev. B* **2003**, *67* (21), 214103.

NL803277G

CNT Membrane Fabrication and Testing

Membranes with high permeability and high selectivity form critical components in applications ranging from molecular separations and drug delivery, to protective garments. The ability to control selectivity and permeability in response to a desired chemical or physical trigger would enhance membrane utility. Membranes with carbon nanotubes (CNTs) as pores present a nanoscale system where improvements can be made to all of the three important membrane properties.

This project explores the following two broad topics:

- Fundamentals of molecular interactions with CNTs and the effects of spatial confinement on the molecular structure, dynamics & transport.
- Active regulation and control of molecular selectivity and transport through carbon nanotubes using highly specific DNA-based molecular gating.

The efforts during the first year of this project at UC Davis focused on the following thrusts: (i) assembly of a multi-component gas permeation system,, (ii) membrane characterization, including single-component gas permeation studies, and (iii) binary gas permeation studies using the multi-component gas permeation system.

(i) Assembly of a multi-component gas permeation system

In order to evaluate the gas separation performance of carbon nanotube (CNT) membranes with a mixed gas, multi-component gas permeation system equipped with a mass spectroscopy (MS) was assembled and installed. A schematic of this system is shown in Figure 1. The present setup employs an inline sampling technique for gas sample extraction from the closed volume and subsequent injection into a MS for concentration analysis. The mixed gas compositions at the feed stream are controlled by mass flow controllers. The retentate gas line from the membrane cell is connected to the back pressure controller maintaining proper stage-cut flow rates to avoid concentration polarization and to sustain a constant mixed gas concentration in the feed gas stream. The permeate and retentate gas streams were analyzed using MS system. In order to obtain the calibration curves for the gas analysis, the MS system calibrated for at least six different gas concentrations (e.g. 20, 40, 50, 60, 80, and 90 %). The gas concentrations in the permeate and retentate stream were obtained by inserting the gas intensity in the calibration curves. The binary gas separation factors of the membrane were calculated based on the MS analysis data of the permeate gases. The gas separation factors, $\alpha_{A/B}$, were calculated by

$$\alpha_{AB} = \frac{y_A/(1-y_A)}{x_A/(1-x_A)} = \frac{y_A/y_B}{x_A/x_B}$$

where x and y are the mole fractions of gas species at the feed and permeate side, respectively.

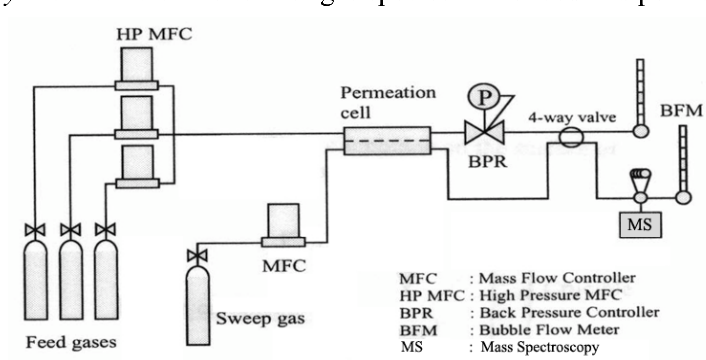

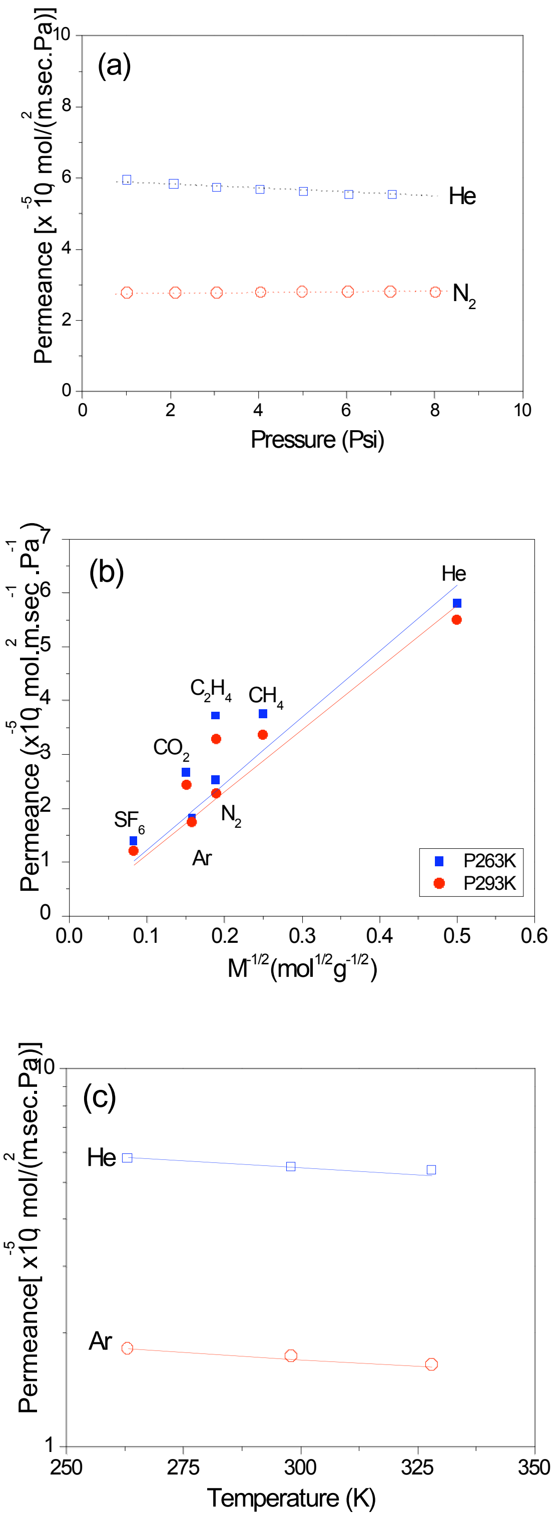

Figure 2. Gas transport properties of CNT/Si_3N_4 membrane. The solid lines are scaled fit predicted by the Knudsen diffusion model at different temperatures. (a) Effect of the pressure drop on the permeance of helium and nitrogen through membrane (b) Single-gas permeance as function of the inverse square root of the molecular weight of the penetrants and (c) Permeation of helium and argon through the membrane at different temperatures.

(ii) Membrane characterization, including single-component gas permeation studies

In order to investigate gas transport through sub-2 nm pore carbon nanotubes (CNT), CNT/Si_3N_4 nano-composite membrane fabricated by a micro-fabrication process has been used.[1] The permeances of $CNTs/Si_3N_4$ composite to all tested gases were measured using the continuous-flow, constant-pressure/variable-volume method. The typical order of gas measurement used in the permeation experiments was helium (He), methane (CH_4), nitrogen (N_2), ethylene (C_2H_4), argon (Ar), carbon dioxide (CO_2), and sulfur hexafluoride (SF_6). The feed pressure was varied from 0 to 8 psig (1.54 atm, 156 kPa) for all tested gases; the permeate pressure was maintained at 0 psig (1.0 atm, 101 kPa). The experimental temperature was varied from 263 to 328 K. The permeate gas flow rate was measured with a soap bubble and a mass flowmeter.

The quality of the CNT membrane was tested by measuring its permeation to helium and nitrogen. Generally, high-quality , pinhole free membranes can be characterized by the absence of viscous flow ($d_p > 50$ nm) and more by Knudsen-like diffusion. For porous membranes that are governed by Knudsen diffusion which is independent of feed pressure, a plot of permeance versus applied pressure should show an independence of feed pressure. Alternatively, the permeance should increase with increasing feed pressure across the membrane when viscous flow takes place. As shown in Figure 2a, the He and N_2 permeance through the nanotube membrane is independent of the pressure drop. This means that there is no viscous flow through any large pinholes or defects. Figure 2b shows the gas permeance of CNT membrane at different temperatures as function of the square root of the reciprocal of the molecular weight of the tested gas, $M^{-1/2}$. The Knudsen flow model (solid line) was scaled to fit the permeance data because the gas permeances of CNT membrane far exceeded the theoretical Knudsen permeance. Strongly absorbing gas species (CO_2, CH_4, and C_2H_4) deviated from the scaled Knudsen permeance due to preferential interactions with CNTs side walls while weakly absorbing gas species (He, N_2, Ar, and SF_6) did not show the deviation. As shown in Figure 2c, the He and Ar permeances decreased as the temperature increased, and showed $T^{-1/2}$ dependence on temperature following the Knudsen diffusion model (solid lines).

(iii) Binary gas permeation studies using the multi-component gas permeation system

Figure 3a and 3b show CH_4/N_2 and CO_2/N_2 gas separation factors of CNT membrane at 263 and 298 K. At 298 K, the separation factors of CNTs membrane are lower than ideal selectivities calculated from single-gas composition studies. For CH_4 and N_2, the low separation factor at 298 K means that the contribution of gas phase flow is much higher than that of surface flow. At 263 K, the separation factor increased because of increased gas adsorption at lower temperature. The CO_2/N_2 selectivity results (Figure 3b) show that the measured separation factors are higher than the theoretical Knudsen

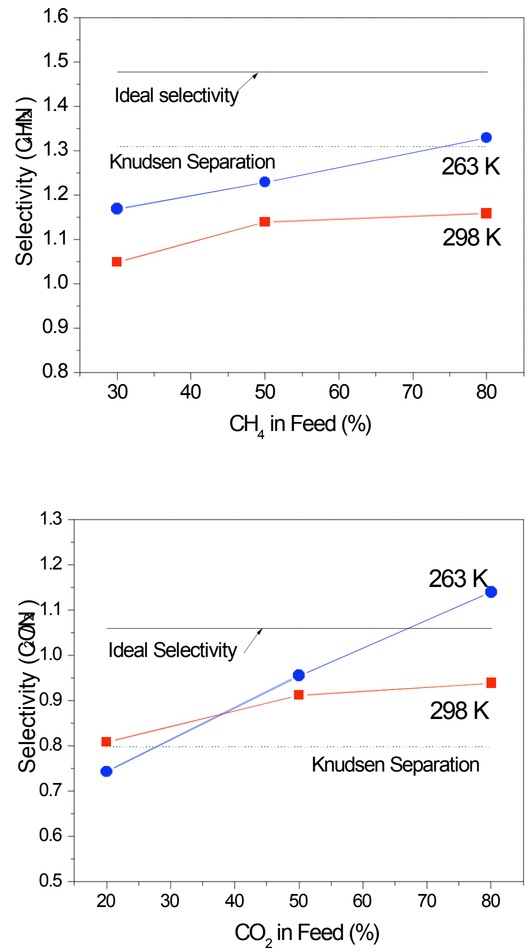

(a)

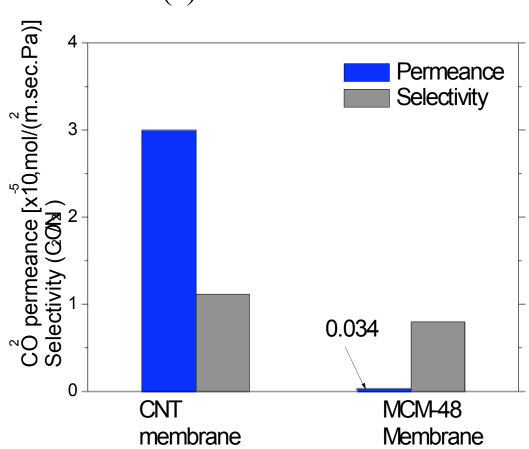

(b)

Figure 3. Bina separation performance of CNT membrane. (a) CH_4/N_2 selectivity at 263 and 298 K, (b) CO_2/N_2 selectivity at 263 and 298 K, and (c) overall CO2/N2 separation performance of CNT membrane comparing with mesoporous MCM-48 membrane with 2 nm pore size and 300 nm thickness.

separation factor indicating the presence of surface diffusion at room temperature. Especially, the CO_2 separation factor at 263 K is even higher than the ideal selectivity due to high amount of CO_2 adsorption to nanotube sidewall. However, the CO_2/N_2 selectivity of nanotube membrane is still lower value for practical CO_2 separation because of lack of optimum pore size for separating CO_2 from CO_2/N_2 mixture. Considering the 1.6 nm of pore size of nanotubes and 0.33 nm of CO_2 monolayer on CNTs sidewall, the effective pore size of the current CNTs membrane in the mixture of CO_2 and N_2 is around 1 nm. At this larger pore diameter, there is no local maximum and minimum of the potential energy curve representing the sorption energy and this is enough space for gas molecules to move freely as in the gases state.[2] Therefore, in order to effectively increase the separation of CO_2 from CO_2/N_2 mixture, the pore diameter near the pore entrance of membrane should be decreased less than 0.6 nm, which is suitable for surface diffusion or capillary condensation, and because the molecular sieving mechanism usually would not take place when the pore diameter is larger than 0.5 nm.

The overall CO_2/N_2 separation performance of CNT membrane compared with mesoporous silica MCM-48 membrane with similar pore size, 2 nm, is shown in Figure 3c. Although the pore density of CNTs membrane (0.05) is smaller than that of mesoprous silica membranes (0.3), the CO_2 permeance of nanotube membrane is higher than mesoporous silica membrane by two orders of magnitude. There are several efforts to increase CO_2 separation factor of mesoporous silica membrane by surface modification of amine functional groups.[3, 4] However, there is a trade-off between the selectivity and permeance. Functionalized silica membrane showed higher selectivity but the permeance decreased by one or two orders of magnitude.

It is supposed that CNT membranes will overcome this limitation. After functionalization of CNT membranes, it is expected that the permeance will be decreased by at most two orders of magnitude. Nonetheless, the modified CNT membranes with high gas selectivities will have similar or higher permeance range compared to current inorganic membrane system.

Chemical force microscopy (CFM) of Si_3N_4/CNT membrane surface (activities)

Transport through the CNT pores is significantly affected by the chemical functionalities at the CNT pore entrance. The silicon nitride/CNT membranes used in our studies underwent a series of etching steps (including ion milling and reactive ion etching) that are supposed to leave the rim of the carbon nanotube pore enriched with hydrophilic functional groups, such as hydroxyl, carbonyl and carboxylic groups. In particular, the presence of ionizable carboxylic groups at the rim should have a significant effect on the charged solute transport.

We have investigated the presence of these ionizable groups using chemical force microscopy titration experiments. The basic concept behind these measurements is to use the pH-dependent interaction forces between the surface and a chemically-modified AFM probe tip to detect changes in the ionization state of the surface chemical functionalities. Typically, these measurements also allow determination of the surface pK_a in a manner analogous to conventional titration experiments.

References

1. Holt, J. K.; Park, H. G.; Wang, Y. M.; Stadermann, M.; Artyukhin, A. B.; Grigoropoulos, C. P.; Noy, A.; Bakajin, O., Fast mass transport through sub-2-nanometer carbon nanotubes. *Science* **2006,** 312, (5776), 1034-1037.
2. Burggraaf, A. J., Single gas permeation of thin zeolite (MFI) membranes: theory and analysis of experimental observations. *Journal of Membrane Science* **1999,** 155, 45-65.
3. Sakamoto, Y.; Nagata, K.; Yogo, K.; Yamada, K., Preparation and CO2 separation properties of amine-modified mesoporous silica membranes. *Microporous And Mesoporous Materials* **2007,** 101, (1-2), 303-311.
4. Kumar, P.; Kim, S.; Ida, J.; Guliants, V. V., Polyethyleneimine-modified MCM-48 membranes: Effect of water vapor and feed concentration on N2/CO2 selectivity. *Industrial & Engineering Chemistry Research* **2008,** 47, (1), 201-208.

Presentations:

- Michigan State University, Science at the Edge Seminar, April 2008
- Panel on emerging technologies for water purification, Water in the Developing World Conference, Stanford, April 2008
- MIT, Seminar, November 2007
- MRS Meeting, Water Symposium, November 2007
- University of Chicago Physics Colloquium, October 2007

University of Illinois Urbana Champaign, WaterCAMPWS Seminar, October 2007